Nonparametric approach for structural dynamics of high-voltage cables

Thomas Berger, Michael Wibmer, Georg Schlüchtermann, Stefan Sentpali, Christian Weißenfels

Angaben zur Veröffentlichung / Publication details:

Berger, Thomas, Michael Wibmer, Georg Schlüchtermann, Stefan Sentpali, and Christian Weißenfels. 2024. "Nonparametric approach for structural dynamics of high-voltage cables." Results in Engineering 22: 102168. https://doi.org/10.1016/j.rineng.2024.102168.

Results in Engineering 22 (2024) 102168

Contents lists available at ScienceDirect

Results in Engineering

journal homepage: www.sciencedirect.com/journal/results-in-engineering

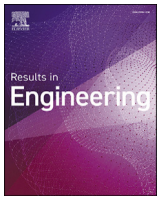

Research paper

Nonparametric approach for structural dynamics of high-voltage cables

Thomas Berger [a,*], Michael Wibmer [a], Georg Schlüchtermann [a], Stefan Sentpali [a], Christian Weißenfels [b]

[a] Department of Mechanical, Automotive and Aeronautical Engineering, Munich University of Applied Sciences HM, Dachauerstr. 98b, 80335, Munich, Germany
[b] Institute of Materials Resource Management, University of Augsburg, Am Technologiezentrum 8, 86159, Augsburg, Germany

ARTICLE INFO

Keywords:
Uncertainty
Nonparametric modelling
Structural dynamics
Vibration
Cable
Random matrix

ABSTRACT

High-voltage cables, as applied in the electro-mobility, are highly complex structures regarding their vibration behaviour. The high complexity leads to considerable uncertainty in models for a finite element method (FEM) simulation, which is shown, for example, in the contact modelling between the strands of the cable. To handle this uncertainty and model the structural dynamic, a nonparametric probabilistic approach (NPPA) with random matrices is used for the first time on high-voltage cables. This novel application of NPPA has an advantage over typical FEM analysis by using a more manageable simulation model and eliminating the need for a complex deterministic simulation model. Initially, the NPPA is analysed and enhanced, with an optimization for the dispersion parameter and a frequency shift introduced as methodological improvements. These enhancements result in a comparable scatter band of the frequency response. Following preliminary studies, the cable's dynamic behaviour is examined through experimental modal analysis, after which the dispersion parameters are computed. The NPPA is then applied to the simplified deterministic model with the calculated dispersion parameters, and a Monte Carlo simulation is done. As a result of this simulation, a scatter band is given. The results from the simulation are then compared to the results of an experiment. It is shown that the frequency response from the experiment is almost always in the inner area of the scatter band. Consequently, this innovative method can be used for a risk evaluation according to the path of the frequency response function and an evaluation of the structural behaviour.

1. Introduction

Cables are essential structures for our lives because they are part of important things like bridges [1], in the energy field as transmission cables [2], or in mobility like electric vehicles [3]. Therefore, it is essential to know how these structures work, especially how the dynamical behaviour works. For example, dynamic behaviour is used to detect bridge damage [4].

Lightweight construction plays a significant role in the development of electric cars. Optimizations are a central aspect in the development phase to enhance the efficiency of electric vehicles and increase passenger comfort. The knowledge of the cables' dynamic behaviour influences the lightweight construction and the acoustic transmission behaviour, which is essential for comfort aspects [5]. Noise below 1000 Hz is mainly transmitted by the solid parts of the car [6]. As cables transmit such noise from sources to the car body, the knowledge of the dynamic behaviour of these cables in the low-frequency range is essential. Often, it is not possible to influence the sources. Therefore, the transfer path must be influenced properly.

Simulations speed up every optimization step and provide a deeper understanding of the structure, so expensive changes in the late development phase can be avoided. In order to run simulations, it is essential to develop models of the real structures. The modelling of the structural vibration of high-voltage cables, such as those used in electric vehicles, is complex. A significant problem is the modelling process of the inner wire, which consists of many strands with complex frictional contact interactions. Measurements [7] show uncertain respectively nonlinear behaviour. Many modelling processes try to model the cable structure with beam elements. For example, there are methods to model the single strands with beam elements [8] or volume elements [9] and contact elements between them. The deterministic modelling approach with beams as strands can not sufficiently represent the complex behaviour

* Corresponding author.
E-mail addresses: thomas.berger@hm.edu (T. Berger), michael.wibmer@hm.edu (M. Wibmer), georg.schluechtermann@hm.edu (G. Schlüchtermann), stefan.sentpali@hm.edu (S. Sentpali), christian.weissenfels@mrm.uni-augsburg.de (C. Weißenfels).

https://doi.org/10.1016/j.rineng.2024.102168
Received 1 December 2023; Received in revised form 29 March 2024; Accepted 19 April 2024
Available online 25 April 2024

of cables [10]. Another method tries to model the whole cable with single beam elements. In [11], for example, this is done by a cosserat rod formulation and in [12], a new beam element is introduced. This element maps the displacement of every strand to the nodes of the element with kinematic formulations. Many publications, such as [13] and [14], deal with static or quasistatic behaviour. The publications rarely consider the structural dynamic of these cables. One of the few publications considering the vibrational behaviour is [15]. This publication shows an extraction of dynamic parameters from experiments and an application in simulation. However, it does not compare a simulation and a real experiment nor perform any modal analysis.

According to the authors' knowledge, the dynamic behaviour of cable structures has not yet been simulative investigated intensively, and the dynamic of high-voltage cables from automotive has not yet been investigated. Therefore, this article will contribute to this fact, and additionally, an NPPA will be used for the first time to consider the uncertainties of the cable systems. The goal is an efficient way to model a high-voltage cable and simulate the dynamic behaviour. Therefore, a simple model can be used in the NPPA, and there is no need for complex modelling, as in the references above. The NPPA handles the complex behaviour of cables with the help of statistical methods. That is a great added value for efficiency and speeds up the simulation time. These aspects make the approach perfect for the increasing speed of the development process, and better decisions can be made in a shorter time. After the simulation, the results will be compared to the real experiment, and the results of this simulation should be close to the experiment. Such a comparison between real experiment results for a high-voltage cable from an automotive and simulative results can not be found in the literature today.

The NPPA, as published by Soize [16] or Adhikari [17], is a method to consider uncertainties in structural systems and is from the field of uncertainty quantification. This approach applies the concepts of random matrices (RMT). Every entry in those matrices is a random variable with a specific distribution. More about random matrices is found in [18]. The advantage of the NPPA is that it can handle not only aleatoric uncertainties (e.g. material parameters, tolerances of the geometry) but also epistemic uncertainties due to the lack of knowledge [19]. The NPPA approach offers the advantage of adjusting matrices from a FEM simulation (such as the stiffness matrix) through the application of RMTs and statistical techniques rather than using more detailed physical models.

The paper is organized as follows. An overview of the NPPA with random matrices and the mean model is shown in Section 2. In the third section, there is a reduced-order strategy for an efficient way to calculate a more significant amount of samples. The fourth section shows the identification of the modal parameters from the experimental modal analysis. The modal analysis gains significant results and is processed in the NPPA. Because the information about the modal analysis is dispersed in more places and is of great importance to the NPPA, the section gives a deeper view of identifying the modal parameters. The preliminary studies of the NPPA are in the fifth section, showing some disadvantages of the method and solution strategies. Section 6 shows the application for the NPPA on a straight cable. There is also a comparison between the experiment and the simulation. A summary and an outlook for further investigations are given at the end of the article.

2. Non-parametric probabilistic approach in structural dynamics

The starting point in structural dynamics is the structural mechanics equation

$$\underline{\mathbf{M}}\ddot{\mathbf{u}}(t) + \underline{\mathbf{D}}\dot{\mathbf{u}}(t) + \underline{\mathbf{K}}\mathbf{u}(t) = \mathbf{f}(t) \tag{1}$$

or in the frequency domain

$$(-\omega^2\underline{\mathbf{M}} + i\omega\underline{\mathbf{D}} + \underline{\mathbf{K}})\mathbf{u}(\omega) = \mathbf{f}(\omega). \tag{2}$$

The matrices $\underline{\mathbf{M}}$, $\underline{\mathbf{D}}$ and $\underline{\mathbf{K}}$ are the system matrices of mass, damping and stiffness of the simulation model. In the following, the simulation model is called the mean model. The system matrices are positive definite on valid boundary conditions, and we will hereafter denote these matrices as $\underline{\mathbf{G}}$.

The goal of the NPPA is to handle not only the parametric uncertainties but also the uncertainties regarding the modelling. Suitable for this purpose is NPPA, according to [19]. This approach can handle both the parametric uncertainties and the non-parametric uncertainties. In this approach, the system matrices are replaced by random matrices $\mathbf{G}$ according to RMT with a specific probability distribution. Soize uses a maximum entropy approach in [16], introduced by Jaynes [20]. In doing so, Soize imposes the following conditions on the distribution: Firstly, the integral over the probability density function has to be one. Secondly, the expectations of the random matrices are the system matrices of the mean model. Thirdly, the moments of the inverse random matrices have to exist. With the maximum entropy approach and the three conditions mentioned above, Soize obtained the probability distribution, the base of the so-called ensembles SG^+ and SE^+. Soize shows in [21] an algebraic formulation for these ensembles. In [17], Adhikari demonstrates that the distribution of Soize is equivalent to a Wishart distribution with the scalar parameter p and the matrix parameter $\mathbf{\Sigma}$. The density function of a random matrix $\mathbf{G}$ of the Wishart distribution is defined as

$$p_G(\mathbf{G}) = \left\{ 2^{\frac{1}{2}np}\Gamma_n\left(\frac{1}{2}p\right)|\mathbf{\Sigma}|^{\frac{1}{2}p}\right\}^{-1} |\mathbf{G}|^{\frac{1}{2}(p-n-1)} e^{-\frac{1}{2}tr(\mathbf{\Sigma}^{-1}\mathbf{G})}. \tag{3}$$

In this equation, $\Gamma(\bullet)$ denotes the multivariate gamma function and $\mathrm{tr}(\bullet)$ is the trace of a matrix.

In the subsequent equation for the parameter p

$$p = n + 1 + \theta_G, \tag{4}$$

the θ_G represented the order of the enforced existing inverse moment ν_G. In the equation for the order of the enforced existing inverse moment ν_G

$$\theta_G = 2\nu_G = \frac{1}{\delta_G^2}\left(1 + \frac{tr(\underline{\mathbf{G}})^2}{tr(\underline{\mathbf{G}}^2)}\right), \tag{5}$$

the dispersion parameter δ_G can be found. This parameter can be considered as a measurement of the accuracy of the simulation model regarding the real structure. It controls the dispersion of the probability model [21]. In the NPPA, every system matrix has its dispersion parameter, and it is used as a scattering parameter of the probability distribution of the random matrices. The dispersion parameter is defined, according to [22], as follows

$$\delta_G^2 = \frac{E\{\|\mathbf{G} - \underline{\mathbf{G}}\|_F^2\}}{\|\underline{\mathbf{G}}\|_F^2}. \tag{6}$$

This equation can be interpreted as a normalized standard deviation. In this equation, $\mathrm{E}\{\bullet\}$ is the expectation operator, and $\|\bullet\|_F$ is the Frobenius norm of a matrix. As shown in [23], every dispersion parameter should be in the range

$$0 < \delta_G < \sqrt{\frac{n+1}{n+5}}, \tag{7}$$

which depends on the size of the system matrices n. In this range, the moments of the inverse random matrices are guaranteed to exist. In [21], it is shown that the dispersion parameters can be determined from an experimental modal analysis. Therefore, the eigenfrequencies, the mode shapes and the modal system matrices of the experiment and the simulation are needed. Furthermore, the dispersion parameter can be calculated from Equation (6) and determined from a maximum likelihood method shown in [24].

In the equation of the parameter Σ, which can be found in Equation (3), the respective system matrix of the mean model is used and can be written as

$$\mathbf{\Sigma} = \frac{1}{p}\underline{\mathbf{G}}. \tag{8}$$

Adhikari postulated in [25] four different criteria on how these parameters p and $\mathbf{\Sigma}$ should be chosen to achieve the best results.

3. Mode superposition method of the mean model

According to [26], the displacements $u(\omega)$ in Equation (2) can be replaced by the eigenvector matrix $\mathbf{\Phi}$ and the modal coordinates $\mathbf{q}(\omega)$ as follows

$$\mathbf{u}(\omega) = \mathbf{\Phi}\mathbf{q}(\omega). \tag{9}$$

The system matrices $\underline{\mathbf{M}}$, $\underline{\mathbf{D}}$ and $\underline{\mathbf{K}}$ will be written

$$\begin{aligned} \underline{\mathbf{M}}_{\mathbf{red}} &= \mathbf{\Phi}^T \underline{\mathbf{M}} \mathbf{\Phi}, \\ \underline{\mathbf{D}}_{\mathbf{red}} &= \mathbf{\Phi}^T \underline{\mathbf{D}} \mathbf{\Phi}, \\ \underline{\mathbf{K}}_{\mathbf{red}} &= \mathbf{\Phi}^T \underline{\mathbf{K}} \mathbf{\Phi}, \end{aligned} \tag{10}$$

and the force vector $\mathbf{f}(\omega)$ will be replaced by

$$\mathbf{f}_{\mathbf{red}}(\omega) = \mathbf{\Phi}^T \mathbf{f}(\omega), \tag{11}$$

which results in the reduced mean model

$$(-\omega^2 \underline{\mathbf{M}}_{\mathbf{red}} + i\omega \underline{\mathbf{D}}_{\mathbf{red}} + \underline{\mathbf{K}}_{\mathbf{red}})\mathbf{q}(\omega) = \mathbf{f}_{\mathbf{red}}(\omega). \tag{12}$$

That reduced mean model can be solved faster because of the fewer degrees of freedom. After solving at every frequency, the modal coordinates $\mathbf{q}(\omega)$ have to be transformed by Equation (9). The solution of the mean model is obtained according to Equation (2).

4. Identification of experimental modal parameters

This section shows the extraction of the eigenfrequencies and eigenvectors from an experimental modal analysis. Furthermore, the structure of the modal system matrices is presented.

4.1. Identification of eigenfrequencies

The eigenfrequencies can be obtained by response functions $H_i(\omega)$, which are from experimental modal analysis. For this purpose, a mode indicator function, e.g. the mode indicator function MIF_1, according to [27], is applied. The idea behind MIF_1 is that the response function is dominated by its imaginary part on locations of eigenfrequencies. That is why break-ins of the MIF_1 are potential locations regarding eigenfrequencies. MIF_1 is defined as

$$\mathrm{MIF}_1 = \frac{\sum_{i=1}^{N} \mathrm{Re}(H_i(\omega))^2}{\sum_{i=1}^{N} |\, H_i(\omega)\,|^2}. \tag{13}$$

According to [27], the condition for MIF_1 is that the response function has a force on the system entry and a displacement or acceleration on the output. As revealed by [28], such a response function is called receptance (output is displacement) or accelerance (output is acceleration). As stated by [27], instead of the outputs mentioned above, if velocity is used as the output parameter, then in Equation (13), the imaginary part has to be replaced by the real part.

Another widely used mode indicator function is the complex mode indicator function CMIF, shown in [29]. CMIF can identify not only eigenfrequencies but also mode shapes. The mode shapes from CMIF are not mass normalized. Therefore, the CMIF is not used in the article's further process.

4.2. Identification of eigenvectors

As shown in [30], the mass-normalized displacement of the mode shape r on the driving point n can be calculated as

$$\Phi_n = \sqrt{|H_{aF,nn}(\omega_{d,r})|\sqrt{D_r^4 + 4D_r^2}}. \tag{14}$$

In this equation, $H_{aF,nn}$ is the response function (accelerance) on the driving point n and the damped eigenfrequency $\omega_{d,r}$. D_r is the damping ratio according to Lehr of the mode shape r. The mass-normalized displacements on the remaining points m are calculated by

$$\Phi_m = \sqrt{D_r^4 + 4D_r^2}\frac{|H_{aF,mn}|}{\Phi_n}. \tag{15}$$

The sign of the imaginary part of the respective response function gives the sign of displacement.

4.3. Modal system matrices

The orthogonality properties of the mass-normalized eigenvectors [28] establish the following relationship between the mass matrix, the eigenvector matrix and the modal mass matrix

$$\mathbf{\Phi}^T\mathbf{M}\mathbf{\Phi} = \begin{bmatrix} 1 & 0 & \dots & 0 \\ 0 & 1 & \ddots & \vdots \\ \vdots & \ddots & \ddots & 0 \\ 0 & \dots & 0 & 1 \end{bmatrix}. \tag{16}$$

The relationship between the stiffness matrix and the modal stiffness matrix is

$$\mathbf{\Phi}^T\mathbf{K}\mathbf{\Phi} = \begin{bmatrix} \omega_1^2 & 0 & \dots & 0 \\ 0 & \omega_2^2 & \ddots & \vdots \\ \vdots & \ddots & \ddots & 0 \\ 0 & \dots & 0 & \omega_k^2 \end{bmatrix}. \tag{17}$$

According to [21], the modal damping matrix can be created with the modal damping value ξ from mode k as

$$\mathbf{D} = \begin{bmatrix} 2\xi_1\omega_1 & 0 & \dots & 0 \\ 0 & 2\xi_2\omega_2 & \ddots & \vdots \\ \vdots & \ddots & \ddots & 0 \\ 0 & \dots & 0 & 2\xi_k\omega_k \end{bmatrix}. \tag{18}$$

5. Preliminary studies on a beam model

This section identifies the weaknesses of the NPPA and how to address them. For this purpose, a simple beam model is used to generate the experimental data. In the experiments, uncertainty is introduced using randomly placed point masses or via the dispersion of Young's modulus. It would analyse how the NPPA behaves with increasing uncertainty. At the end of the chapter, two improvements of the weaknesses identified in the analysis are pointed out.

5.1. Experimental data from a FEM model

A FEM model (see Fig. 1) creates the experimental data. The model consists of 90 2D-Euler-Bernoulli beam elements and is mounted turnable on its ends. Furthermore, point masses are applied randomly (according to uniform distribution) on the beam. These point masses have a mass of 0.5 % for the investigation of small uncertainty or 8.0 % for more significant uncertainty in the first two investigations. The point masses were omitted in the third investigation, and only Young's modulus was variated to investigate the uncertainty of the stiffness.

The model was harmonically excited by a force of 1 N on the location $x = 1/3l$. All model parameters are listed in Table 1. For each investigation, there were 500 samples created.

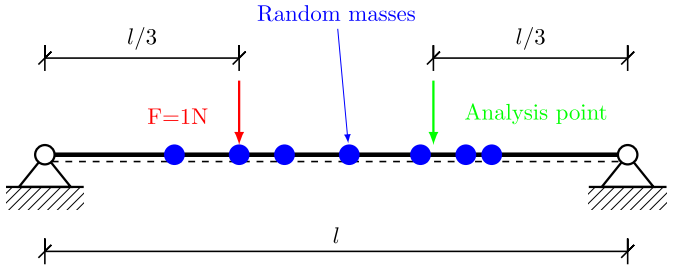

Fig. 1. Model with randomly applied point masses to create experimental data with uncertain behaviour.

Table 1
Model parameters for NPPA mean model and experimental data model.

Parameter	Value
Density ρ	7850.000 kg m^{-3}
Length l	0.500 m
Diameter D	0.015 m
Young's modulus E	2.1×10^{11} N m^{-2}

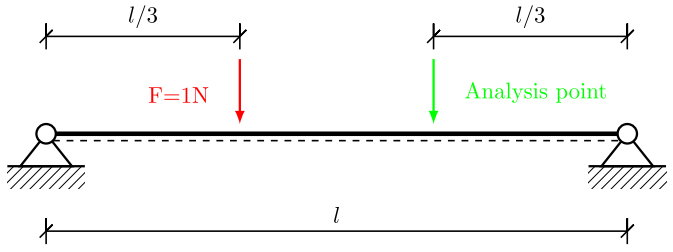

Fig. 2. Mean model used for the NPPA in the preliminary studies.

5.2. Mean model

The NPPA mean model was analogous to [21], created with an Euler-Bernoulli beam model (see Fig. 2). This beam with the length of l was hinged on his ends. The modal system matrices of the NPPA mean model in section 3 are defined as

$$\underline{\mathbf{M}}_{\mathbf{red}} = \begin{bmatrix} \underline{\rho}_l & 0 & \dots & 0 \\ 0 & \underline{\rho}_l & \ddots & \vdots \\ \vdots & \ddots & \ddots & 0 \\ 0 & \dots & 0 & \underline{\rho}_l \end{bmatrix},$$

$$\underline{\mathbf{D}}_{\mathbf{red}} = \begin{bmatrix} 2\xi\underline{\rho}_l\omega_1 & 0 & \dots & 0 \\ 0 & 2\xi\underline{\rho}_l\omega_2 & \ddots & \vdots \\ \vdots & \ddots & \ddots & 0 \\ 0 & \dots & 0 & 2\xi\underline{\rho}_l\omega_n \end{bmatrix}, \tag{19}$$

$$\underline{\mathbf{K}}_{\mathbf{red}} = \begin{bmatrix} \underline{\rho}_l\omega_1^2 & 0 & \dots & 0 \\ 0 & \underline{\rho}_l\omega_2^2 & \ddots & \vdots \\ \vdots & \ddots & \ddots & 0 \\ 0 & \dots & 0 & \underline{\rho}_l\omega_n^2 \end{bmatrix}.$$

Here $\underline{\rho}_l = \rho A$ with $A = d^2/4\pi$ the mean density per length, ξ the modal depending on ratio and ω_α the eigenfrequency of the respective mode. The following equation can calculate the eigenfrequency of the respective mode

$$\omega_\alpha = \sqrt{\frac{\underline{k}}{\underline{\rho}_l}} \left(\frac{\alpha\pi}{l}\right)^2, \quad \alpha = 1, 2, \dots, n. \tag{20}$$

The mean bending stiffness $\underline{k}$ is the product of Young's modulus and the geometrical moment of inertia I of a circle with diameter d and written as

Table 2
Investigation 1: Dispersion parameters.

Dispersion parameter	Normalized standard deviation	Max-Likelihood method
Mass	0.0536	0.0522
Stiffness	0.0001	0.0001
Damping	0.0246	0.0243

$$\underline{k} = EI = E\frac{\pi d^4}{64}. \tag{21}$$

The modes of the respective eigenfrequency are defined as

$$\upsilon_\alpha(x) = \sqrt{\frac{2}{l}} \sin\left(\frac{\alpha\pi}{l}x\right), \quad \alpha = 1, 2, \dots, n. \tag{22}$$

The modal force vector $\mathbf{f}_{\mathbf{red}}(\omega) = (f_1(\omega), \dots, f_n(\omega))$ is created by

$$f_\alpha(\omega) = \underline{g}(\omega)\upsilon_\alpha(x_0), \quad \alpha = 1, 2, \dots, n. \tag{23}$$

The approach from Equation (9) is written here as

$$u(x, \omega) = \sum_{\alpha=1}^{n} q_\alpha(\omega)\underline{\upsilon}_\alpha(x). \tag{24}$$

Here is $\mathbf{q} = (q_1(\omega), \dots, q_n(\omega))$ the solution of Equation (12). The model parameters of the mean model are listed in Table 1.

5.3. Investigation 1: point masses with 0.5% mass of the beam mass

At first, the experimental modal system matrices, according to Section 4, have to be created to calculate the dispersion parameters. For this purpose, the first six modes are sufficient. As shown in [24], the modal system matrices must be transformed for valid comparison in the vector basis of the mean model. Subsequently, the dispersion parameters were calculated by Equation (6), respectively shown in [24] and also with the maximum likelihood method from [24]. The calculated dispersion parameters are listed in Table 2.

With these dispersion parameters (normalized standard deviation), 500 mass, stiffness and damping matrix were created according to the SG$^+$ respectively to the SE$^+$ ensemble from the NPPA. Equation (12) is solved for the solution of the NPPA in the frequency band 0 to 5000 Hz.

In Fig. 3, the comparison of the mean values of all data points between experimental data and NPPA data is shown. Furthermore, the scatter bands where 90% of the data points lie are drawn. Fig. 4 indicates the distribution of the first two eigenfrequencies and the amplitude of the response function at the location of the eigenfrequency.

As recognized in Fig. 3, the mean values differ from each other. Also, the scatter bands show differences. However, the scatter band of the experimental data is almost always in the area of the scatter band of the NPPA data. That means doing a risk evaluation of the response function with the simplified mean model is possible.

The distribution of the first two eigenfrequencies (see Fig. 4) shows different positions of the mean value between the experimental data and the NPPA data. The reason for this is the modelling differences between experimental model and the NPPA mean model. The NPPA mean model has less mass than the experimental model. Therefore, the position of the mean value of the eigenfrequencies is different. This modelling error leads to a broader distribution of the eigenfrequencies of the NPPA because the NPPA attempts to integrate the experiment's frequency band in the NPPA band.

5.4. Investigation 2: point masses with 8.0% mass of the beam mass

As in the preceding investigation in Section 5.3, the dispersion parameters were calculated similarly. The calculated dispersion parameters δ are listed in Table 3. It shows a difference between the mass dispersion parameter δ_M calculated by the normalized standard deviation and the one of the maximum likelihood method.

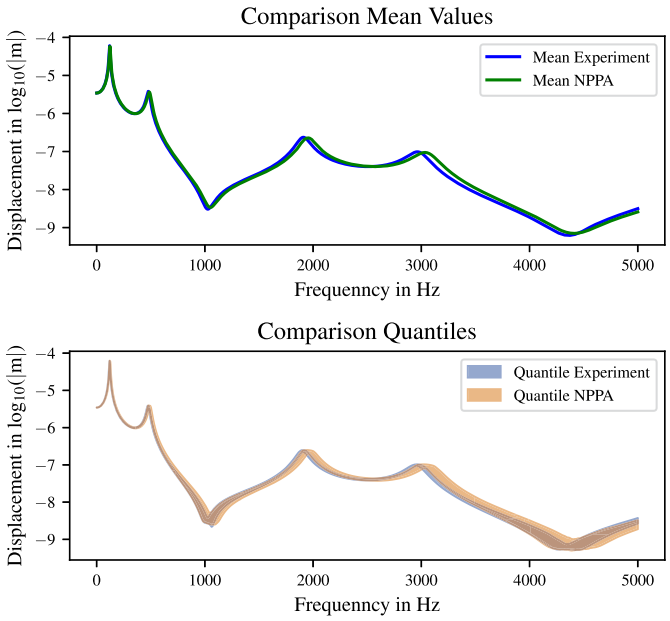

Fig. 3. Investigation 1: Comparison of the mean values and the quantiles from the samples of the experimental data and the NPPA data.

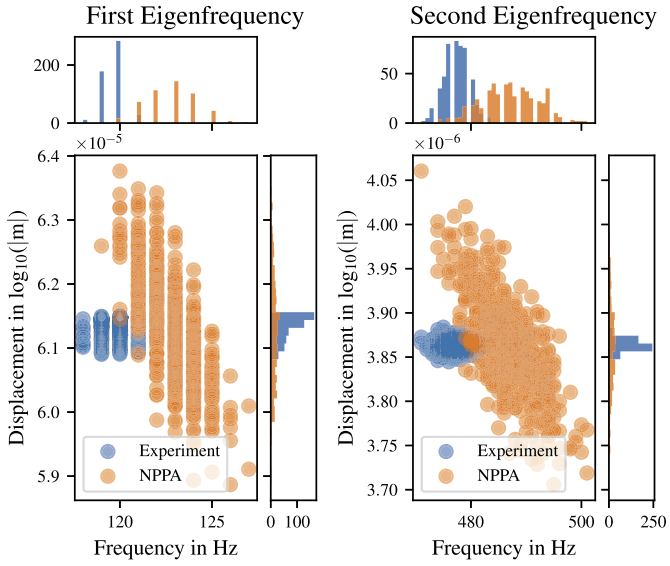

Fig. 4. Investigation 1: Comparison of the first two eigenfrequency distributions between the experimental data and the NPPA data.

Table 3
Investigation 2: Dispersion parameters.

Dispersion parameter δ	Normalized standard deviation	Max-Likelihood method
Mass δ_M	0.7764	0.5711
Stiffness δ_K	0.0091	0.0090
Damping δ_D	0.2864	0.2545

Similar to Section 5.3, 500 samples were created, and Equation (12) was solved for the same frequency band. Fig. 5 shows the experimental and NPPA data's mean values and scatter bands. Compared to investigation 1, there are more noticeable differences between the two data sets. The NPPA data has a broader scatter band than the experimental data for most ranges. Thus, the NPPA data does not match the experimental data well.

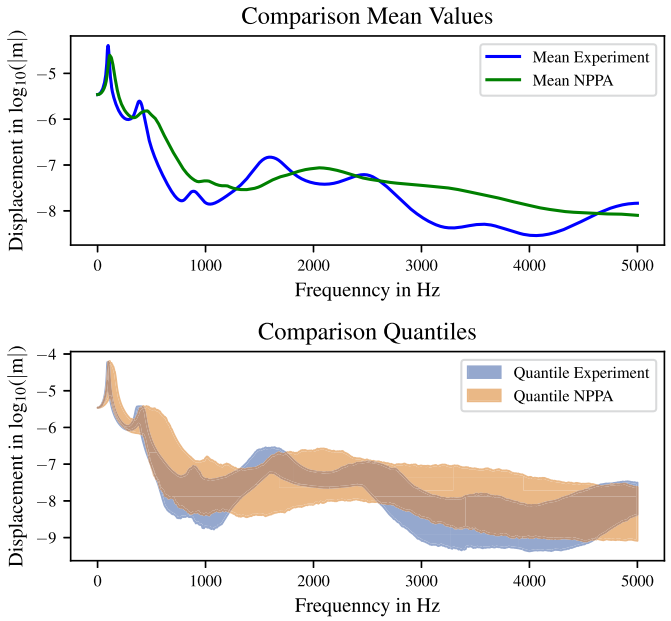

Fig. 5. Investigation 2: Comparison of the mean values and the quantiles from the samples of the experimental data and the NPPA data.

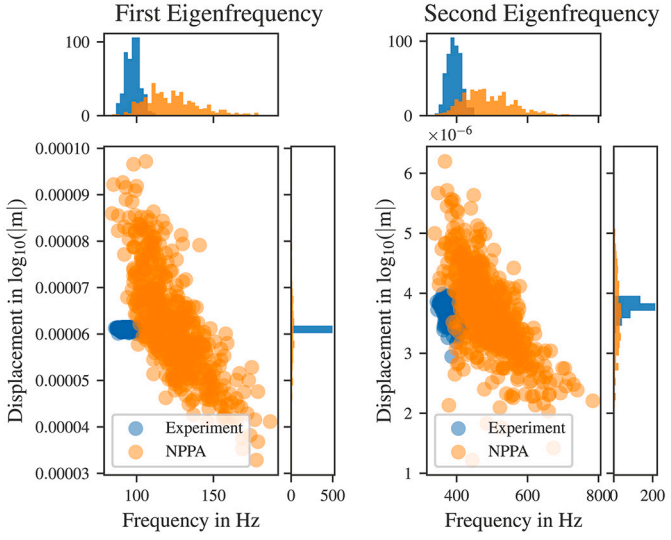

Fig. 6. Investigation 2: Comparison of the first two eigenfrequency distributions between the experimental data and the NPPA data.

As in Section 5.3, the distribution of both first eigenfrequencies of the NPPA (see Fig. 6) have a broader distribution, and the mean value of the eigenfrequencies is at different locations.

5.5. *Investigation 3: variation of the Young's modulus*

Young's modulus is variated in this section, and the point masses were omitted. The randomly generated values for Young's modulus were created by a normal distribution with a mean value of 210000 N/mm^2 and a standard deviation of 21000 N/mm^2. The dispersion parameters and the response functions were created the same way as in the preceding investigations. Unlike the investigation in Section 5.4, there is no mismatch between the dispersion parameters of the different calculation methods shown in Table 4.

Furthermore, the scatter band of the NPPA data is smaller than that of the experimental data, as shown in Fig. 7. Fig. 8 shows the distribution of both first eigenfrequencies. Here, there is a difference between

Table 4
Investigation 3: Dispersion parameters.

Dispersion parameter δ	Normalized standard deviation	Max-Likelihood method
Mass δ_M	0.0108	0.0107
Stiffness δ_K	0.1029	0.1052
Damping δ_D	0.0524	0.0529

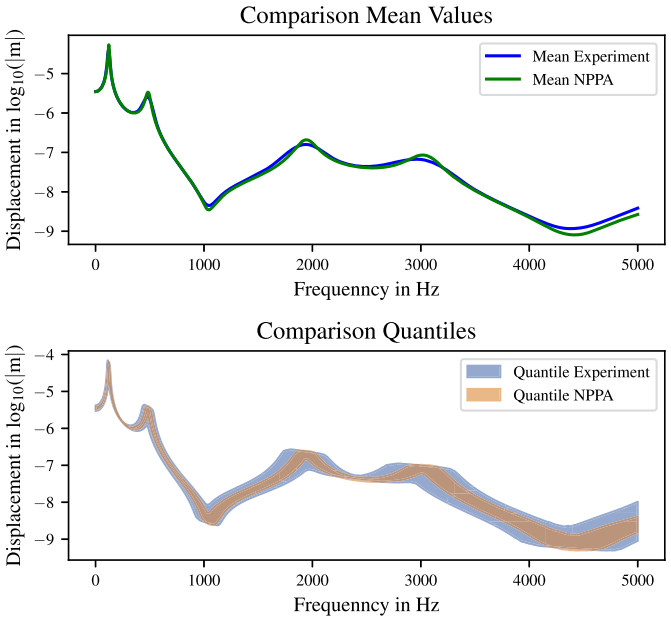

Fig. 7. Investigation 3: Comparison of the mean values and the quantiles from the samples of the experimental data and the NPPA data.

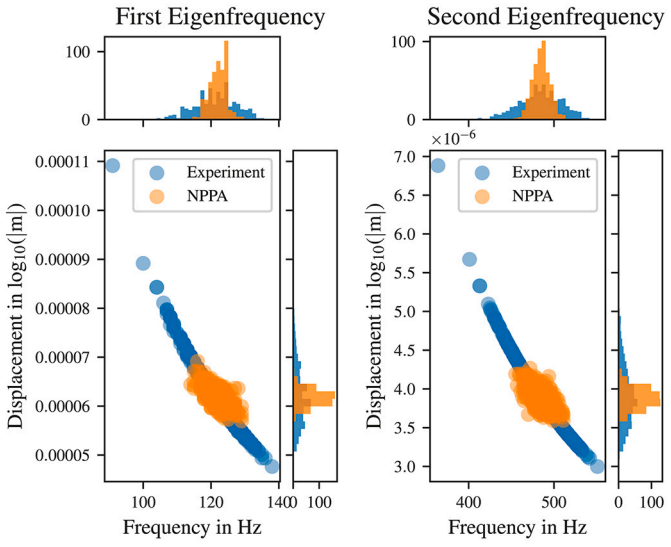

Fig. 8. Investigation 3: Comparison of the first two eigenfrequency distributions between the experimental data and the NPPA data.

this study and the other studies. In this study, the eigenfrequency distribution of the NPPA data is narrower than the experimental data.

5.6. Dispersion parameter optimization

As Section 5.3 and Section 5.4 show, the choice of the dispersion parameter by the normalized standard deviation is worsening with increasing uncertainty. Either the scatter band of the NPPA data is too

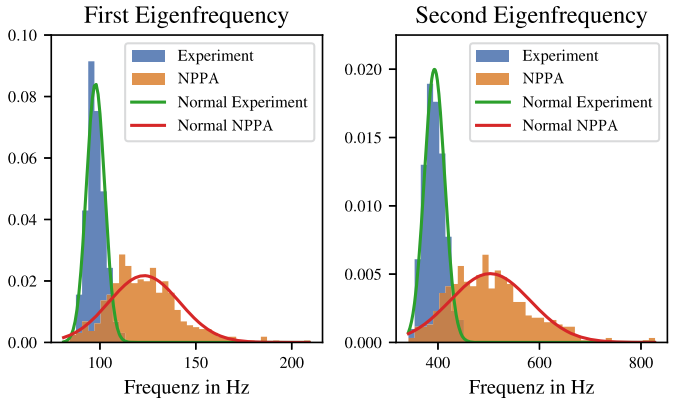

Fig. 9. Random masses 8.0%: Comparison of the first two eigenfrequency distributions and fitted normal distributions between experiment and NPPA before the optimization.

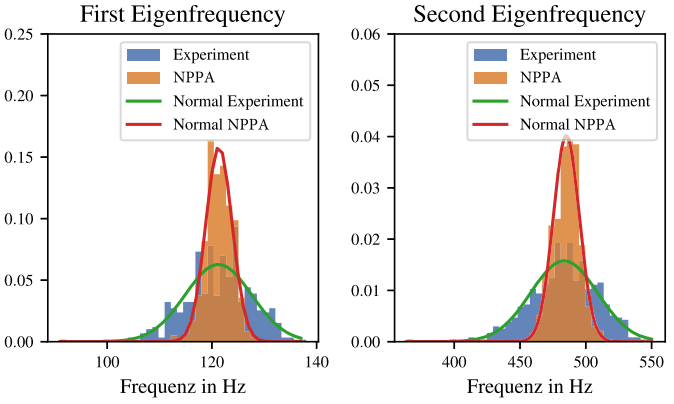

Fig. 10. Variation Young's modulus: Comparison of the first two eigenfrequency distributions and fitted normal distributions between experiment and NPPA before the optimization.

broad or narrow. In the cases of the preliminary studies, many experimental data are available. So, the distribution of eigenfrequencies can be approximated by a probability distribution (see Fig. 9 and Fig. 10). For the two preceding investigations of Section 5.4 and Section 5.5, the distribution is approximated by a standard normal distribution. With the n standard deviations of the approximated distributions of the experimental data and the NPPA data, the optimization problem

$$\min_{\delta_M,\delta_K} \quad \sum_{i=1}^{n} (\sigma_{exp,i} - \sigma_{sim,i}(\delta_M, \delta_K))^2 \tag{25}$$

can be solved. For this investigation, $n = 2$ involves the first two standard deviations of the eigenfrequencies. The number of eigenfrequencies involved could be chosen arbitrarily. For the case of Section 5.4, the optimization parameter is the dispersion parameter of the mass. In the case of Section 5.5, the dispersion parameter of the stiffness is chosen as the optimization parameter. In the general case, both parameters have to be optimized. One way to optimize the damping dispersion parameter is by examining the amplitude distribution of the response function at the locations of the eigenfrequencies and approximating it with a probability distribution. The dispersion parameter of the damping can also optimize the deviation of the chosen distribution. That is not done in this study.

The distributions of the eigenfrequencies for both cases after the optimization are shown in Fig. 11 and Fig. 12. The deviation of both distributions is more similar after the optimization than before.

The optimized dispersion parameters are listed in Table 5. For the case of investigation 2 in Section 5.4, the value of the dispersion param-

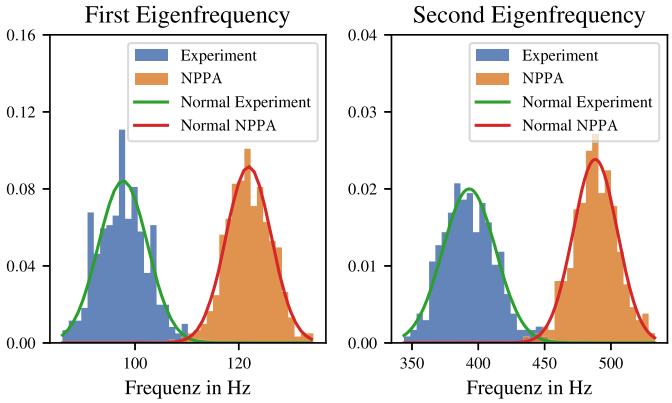

Fig. 11. Random masses 8.0%: Comparison of the first two eigenfrequency distributions and fitted normal distributions between experiment and NPPA after the optimization.

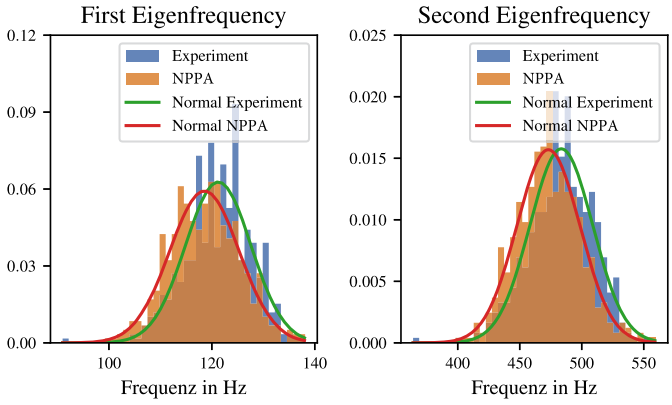

Fig. 12. Variation Young's modulus: Comparison of the first two eigenfrequency distributions and fitted normal distributions between experiment and NPPA after the optimization.

Table 5
Dispersion parameters of studies random masses 8.0% and variation Young's modulus after optimization.

Dispersion parameter	Random masses 8.0%	Variation Young's modulus
Mass	0.1854	0.0108
Stiffness	0.0091	0.2653
Damping	0.2864	0.0524

eter decreases as expected. For the case of investigation 3 in Section 5.5, the value of the dispersion parameter increases as expected.

The comparison of the mean values and the scatter bands for the case of Section 5.4 is shown in Fig. 13. The courses are almost similar. However, the mean values of the eigenfrequencies are not at the exact location. For that reason, the frequency shift, which is presented in the next section, can make improvements.

The scatter bands and mean values for Section 5.5 are compared in Fig. 14, showing a good approximation between experimental data and NPPA data.

5.7. Frequency shift

As seen in Fig. 11, the location of the mean between the experiment and NPPA can be very different. To improve this situation, we will calculate the mean value of the ratios of the eigenfrequency ratios, denoted as r_ω, by the following equation

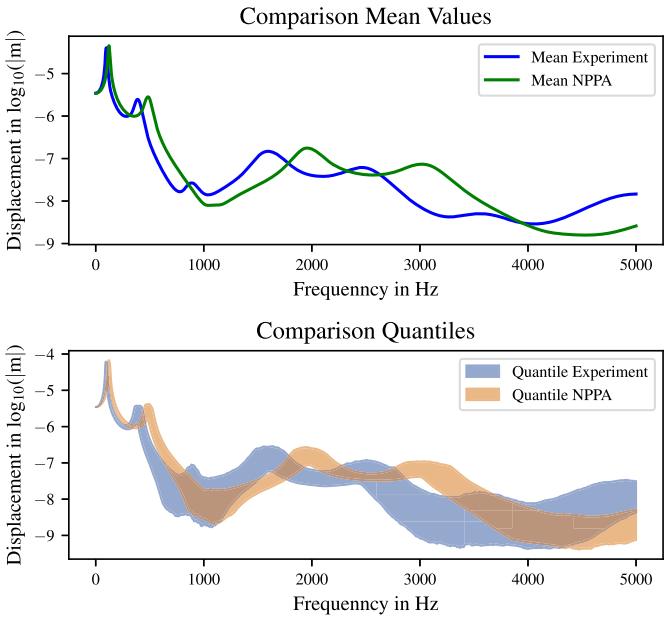

Fig. 13. Random masses 8.0%: Comparison of the mean values and the quantiles from the samples of the experiment and the NPPA after optimization.

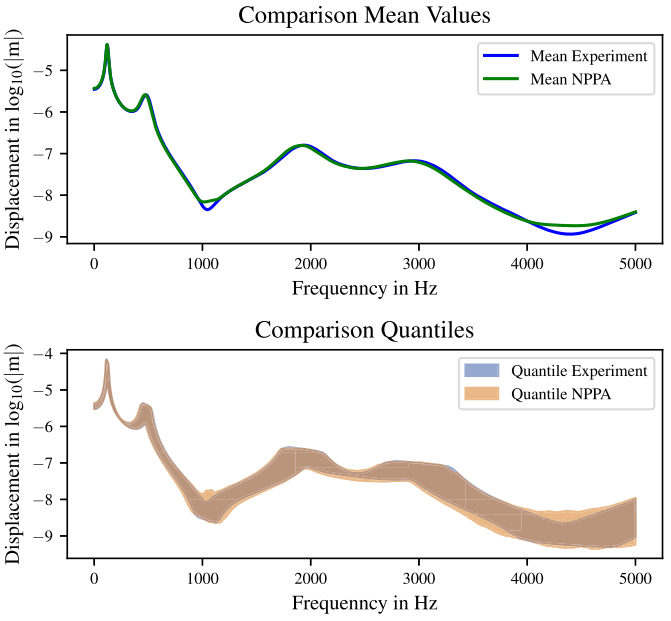

Fig. 14. Variation Young's modulus: Comparison of the mean values and the quantiles from the samples of the experiment and the NPPA after optimization.

$$r_\omega = \frac{1}{n}\sum_{i=1}^{n}\frac{\bar{\omega}_{exp,i}}{\bar{\omega}_{sim,i}}. \tag{26}$$

Analogous to the one-degree-of-freedom system, the eigenfrequency is calculated by

$$\omega_{new} = r_\omega\sqrt{\frac{k}{m}} = \sqrt{\frac{k}{c\cdot m}}. \tag{27}$$

The approach is to modify the mass matrix by multiplying with the corrector value c to change the location of the mean value of the eigenfrequency distributions. In the case of Section 5.4, the corrector value with the two first eigenfrequencies implied was $c = 1.54$.

The distribution of the first two eigenfrequencies of the model with the modified mass matrix is shown in Fig. 15. Fig. 16 shows the compar-

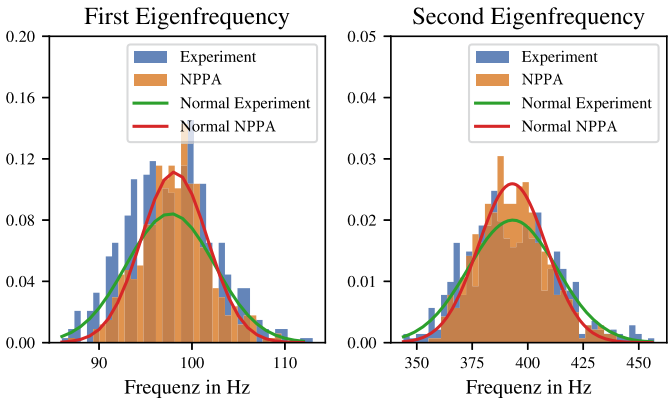

Fig. 15. Random masses 8.0%: Comparison of the first two eigenfrequency distributions and fitted normal distributions between experiment and NPPA after frequency shift.

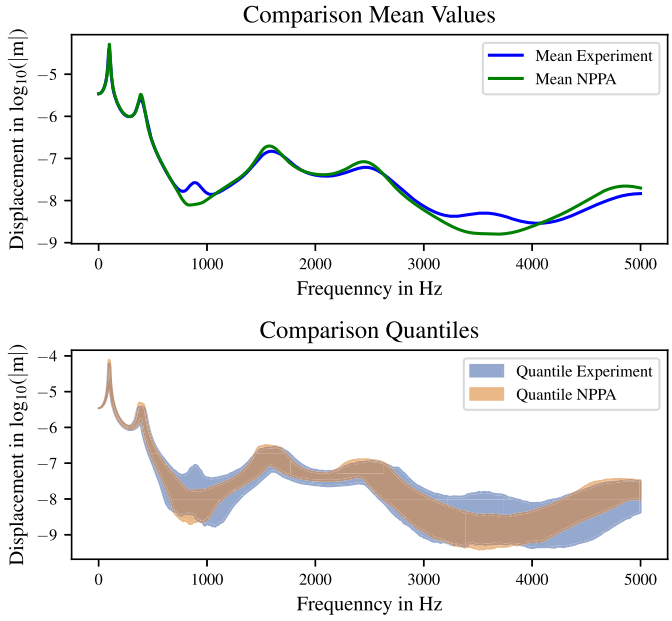

Fig. 16. Random masses 8.0%: Comparison of the mean values and the quantiles from the samples of the experiment and the NPPA after frequency shift.

ison of the mean values and the scatter bands. In the two charts, there is an improvement in the location of the mean values of the eigenfrequencies to see, and the scatter bands match better.

6. Application of non-parametric approach for high-voltage cable

This section discusses the application of NPPA to a high-voltage cable used in the automotive industry. First, the experimental measurements on the high-voltage cable are described. Then, the mean value model for NPPA is presented, and finally, the implementation of NPPA is shown and evaluated. For this purpose, the mean model is compared to the experiment, and it will be checked if the experiment is in the scatter band of the NPPA.

6.1. Experiment

For the determination of the response functions, according to the experimental setup from [31], the high-voltage cable (type: FHLR2GCB2G, cross-section: 35 mm^2) was installed between two impedance masses and elastically mounted on one side. The impedance masses functioned as a fixed boundary condition due to the mass difference between the cable and the impedance masses. Acceleration sensors were installed along the cable and on the masses. The schematic structure of the experiment is shown in Fig. 17. During the implementation of the experiment, the cable was excited transverse to the longitudinal cable axis on positions 3 and 4 and in the longitudinal direction to the cable on the upper mass by a hammer blow.

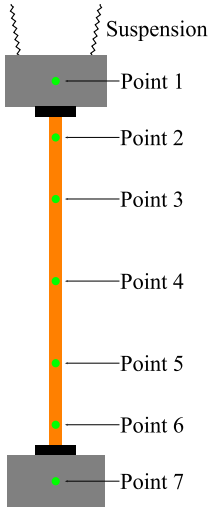

Fig. 17. Schematic structure of the experimental setup with applied acceleration sensors on points 1 to 7.

Table 6
Eigenfrequencies of the cable.

Label	Frequency in Hz
First bending eigenfrequency	36.50
Second bending eigenfrequency	97.50
Third bending eigenfrequency	209.50
Eigenfrequency longitudinal wave	1105.50

6.2. Response function

The response functions from the experiment at positions 3, 4 and 5 can be found in blue drawn in Fig. 21. The response functions on the left side are the ones that are excited on position 4 transverse to the longitudinal cable axis. Those excited on position 3 transverse to the longitudinal cable axis are on the right side.

6.3. Eigenfrequencies

The eigenfrequencies of the cable can be detected by the MIF_1 function, which is described in Section 4. This function is shown in Fig. 18. The second, third and fourth break-ins are the positions of the first three bending eigenfrequencies of the cable. The MIF_1 function for the excitement in the longitudinal direction gives an idea of the position of the longitudinal wave eigenfrequency. The eigenfrequency is not on the heaviest break-in but on the smaller break-in before at 1105.50 Hz. This also confirmed a comparison of the displacements at the two frequencies. A listing of all eigenfrequencies of the cable is shown in Table 6.

6.4. Mean model

As mentioned before, the impedance masses can be seen as fixed boundaries. Because of that, a two-sided fixed beam, according to the Timoshenko beam theory, functioned as a mean model. This beam was discretized with 252 elements. Analytical relationships from [32] were used to get the model parameters. The Young's modulus could

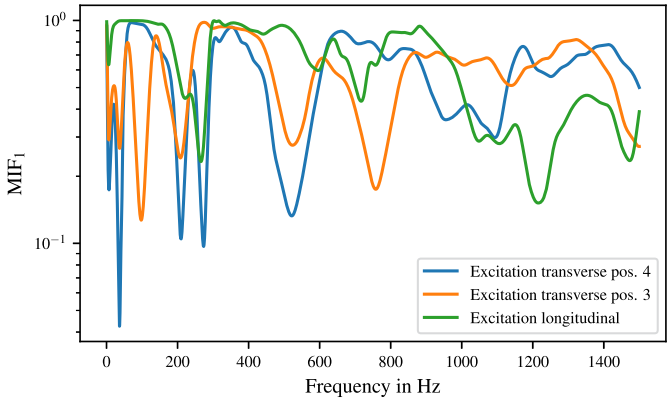

Fig. 18. Mode indicator functions MIF_1 of the experimental data.

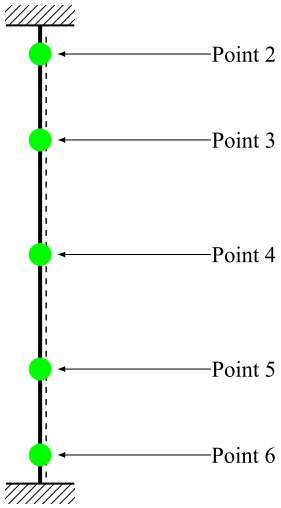

Fig. 19. Mean model of the high-voltage cable used for the NPPA.

be determined from the relationship of the eigenfrequency of the first longitudinal wave on a two-sided fixed beam

$$\omega = \frac{\pi}{l}\sqrt{\frac{E}{\rho}} \tag{28}$$

with the cable length l, the eigenfrequency of the longitudinal wave from the experiment and the density appropriate to the mass. The geometrical moment of inertia of the beam could be determined from the equation of the first bending eigenfrequency of a two-sided fixed beam

$$\omega = (\beta l)^2\sqrt{\frac{EI}{\rho A l^4}}. \tag{29}$$

Thereby βl for the first eigenfrequency is

$$\beta l = 4.73 \tag{30}$$

and A the circular cross-section of the cable with diameter D. As a damping model, constant structural damping is used with a value of $g = 0.6$. With the selection of this value, the response functions are all in the same region. The schematic structure of the mean model is shown in Fig. 19. All parameters for the models are listed in Table 7. The force of the experiment is used as excitation on positions 3 and 4.

6.5. Mode shapes and dispersion parameters

The experiment's mode shapes are needed to calculate the dispersion parameters. The mode shapes can be calculated from Equation (14) and Equation (15). For this calculation, the response functions of the driving point, the remaining points, and the damping ratio, according to Lehr, are needed. The value of this damping ratio was determined with a damped modal analysis and a harmonic response analysis of the mean model. For this purpose, the response function of this simulation with a constant structural damping value of 0.6 was compared with the experiment. For this value, the graphs are all in the same region. From the damped modal analysis with this constant structural damping value, we get the damping ratio of 0.2669. The calculated mode shapes of the experiment and the mean model are shown in Fig. 20.

Table 7
Parameters of the mean model of the high-voltage cable.

Parameter	Value
Density ρ	3939.4000 kg/m^3
Cable length l	0.4980 m
Cable diameter D	0.0144 m
Young's Modulus E	4.7760×10^9 N m^{-2}
Geometrical moment of inertia I	8.6815×10^{-10} m^4
Constant structural damping g	0.6

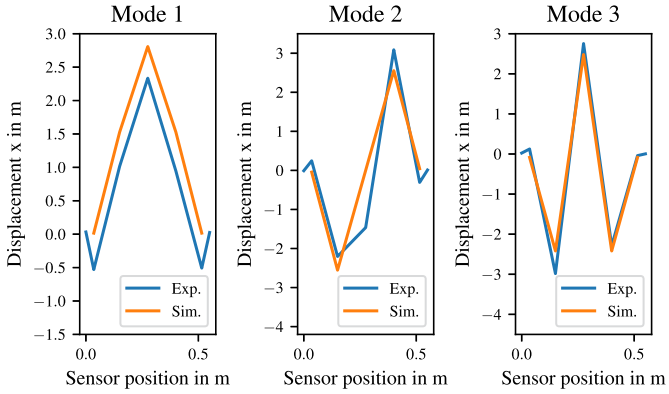

Fig. 20. Comparison of the first three mode shapes between the experiment and the simulation.

Table 8
Dispersion parameters for the high-voltage cable.

Dispersion parameters	Value
Mass δ_M	0.4163
Damping δ_D	0.4292
Stiffness δ_K	0.6655

According to Section 4, the modal system matrices were created from the experiment's determined eigenfrequencies, the mean model's eigenfrequencies and the modal damping ratio. For the reason of comparison, the modal system matrices of the experiment have to be transformed with the eigenvector matrix from the mean model and the experiment in the vector basis from the mean model. This is shown in [21]. After that, the dispersion parameters were calculated according to Equation (6). The dispersion parameters are listed in Table 8. With the dispersion parameters from Table 8 and the system matrices of the mean model, 500 samples according to the SG^+ respectively SE^+ ensemble were created for the mass, stiffness and damping matrices. After that, the response functions at the measurement points were determined with the modal superposition from Section 3 for excitation on positions 3 and 4. Fig. 21 shows all the samples drawn in yellow. In addition to that, the borders of the scatter band are drawn red dashed. 90% of all solutions are between these borders. Furthermore, the response function of the experiment is in blue, and the response function of the mean model is in orange.

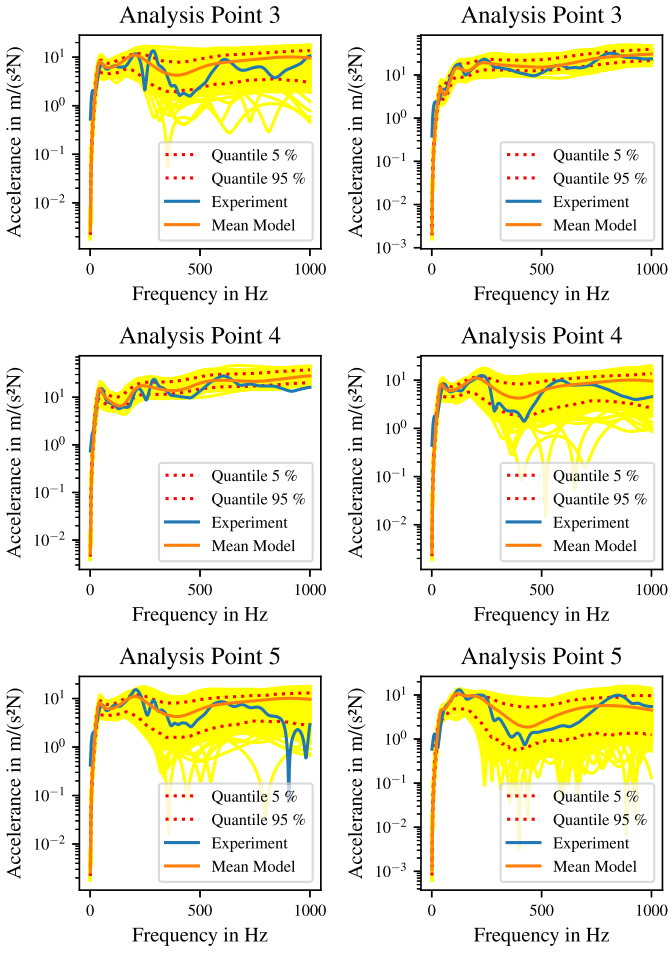

Fig. 21. Comparison of the frequency response between experiment and simulation and the quantiles from the created samples of the simulation (left: excitation point 4; right: excitation point 3).

Fig. 21 shows that the response functions from the experiment are almost in the area of the scatter band. Therefore, the scatter bands are suitable for risk evaluation according to the positions of the response function for a straight high-voltage cable. It also shows that the mean model matches the first two eigenfrequencies well.

7. Conclusion and outlook

This work has shown that the nonparametric approach with random matrices, a simplified mean model and modal superposition can efficiently map the experimental response function of a high-voltage cable by a scatter band. This scatter band can be used for a risk evaluation regarding the maxima and minimal values of the response function, and the structural, dynamical behaviour of the cable can be determined.

Furthermore, the preliminary studies showed that with increasing uncertainty and dispersion parameters, the scatter bands and the distribution of the eigenfrequencies do not match together. Therefore, a dispersion parameter optimization method is shown. The dispersion parameter optimization method can be done if sufficient data is available. Also, a frequency shift is shown. These two tools can make improvements regarding the approximation of the response functions.

The investigations of this article show a strong dependency on the quality of the mean model. If the mean model is far away from reality, the approach will not create a good solution, and the borders of Equation (7) can not be held.

In order to calculate different cable paths in the future, utilizing the method demonstrated here on element matrices instead of global system matrices would be beneficial. A workflow that involves performing an experimental modal analysis on a cable sample and applying the obtained dispersion parameters, along with a nonparametric approach, to a single finite element could be developed. However, it has to be investigated if the distribution obtained from the maximum entropy approach is still valid for a single element that is then assembled.

CRediT authorship contribution statement

Thomas Berger: Conceptualization, Data curation, Formal analysis, Investigation, Methodology, Software, Validation, Visualization, Writing – original draft, Writing – review & editing. **Michael Wibmer:** Conceptualization, Funding acquisition, Project administration, Resources, Supervision, Writing – review & editing. **Georg Schlüchtermann:** Conceptualization, Supervision, Writing – review & editing. **Stefan Sentpali:** Supervision, Writing – review & editing. **Christian Weißenfels:** Supervision, Writing – review & editing.

Declaration of competing interest

The authors declare that they have no known competing financial interests or personal relationships that could have appeared to influence the work reported in this paper.

Data availability

Data will be made available on request.

Acknowledgements

The authors are grateful to the Bavarian Ministry of Science and the Arts for supporting the research project MSSKW, from which this work has resulted. They also thank the referees for their helpful comments.

References

[1] S.A. Derseh, T.A. Mohammed, Bridge structures under progressive collapse: A comprehensive state-of-the-art review, Results Eng. 18 (2023) 101090, https://doi.org/10.1016/j.rineng.2023.101090.

[2] A. Garrod, S. Neda Hussain, A. Ghosh, S. Nahata, C. Wynne, S. Paver, An assessment of floating photovoltaic systems and energy storage methods: A comprehensive review, Results Eng. 21 (2024) 101940, https://doi.org/10.1016/j.rineng.2024.101940.

[3] S. Ramer, D. Winkler, Cable Design for Hybrid Electric/Fuel Cell Vehicles as it Relates to OEM and Harness Maker Requirements, in: SAE World Congress & Exhibition, 2009, pp. 2009–01–1096.

[4] R. Niyirora, W. Ji, E. Masengesho, J. Munyaneza, F. Niyonyungu, R. Nyirandayisabye, Intelligent damage diagnosis in bridges using vibration-based monitoring approaches and machine learning: A systematic review, Results Eng. 16 (2022) 100761, https://doi.org/10.1016/j.rineng.2022.100761.

[5] R. Guo, L.-J. Zhang, J. Zhao, H. Zhou, Interior structure-borne noise reduction by controlling the automotive body panel vibration, Proc. Inst. Mech. Eng., Part D, J. Automob. Eng. 226 (7) (2012) 943–956, https://doi.org/10.1177/0954407011433119.

[6] T.C. Lim, G.C. Steyer, Hybrid Experimental-Analytical Simulation of Structure-Borne Noise and Vibration Problems, in: Automotive Systems, in: International Congress & Exposition, 1992, p. 920408.

[7] D. Manfredo, V. Dörlich, J. Linn, M. Arnold, First Steps in Data Based Constitutive Modelling of Inelastic Effects in Composite Cables Using Preisach Hysteresis Operators, in: Proceedings of the 10th ECCOMAS Thematic Conference on MULTIBODY DYNAMICS, Budapest University of Technology and Economics, Online, 2021, pp. 380–390.

[8] S. Lalonde, R. Guilbault, F. Légeron, Modeling multilayered wire strands, a strategy based on 3D finite element beam-to-beam contacts - Part I: Model formulation and validation, Int. J. Mech. Sci. 126 (2017) 281–296, https://doi.org/10.1016/j.ijmecsci.2016.12.014.

[9] R. Judge, Z. Yang, S. Jones, G. Beattie, Full 3D finite element modelling of spiral strand cables, Constr. Build. Mater. 35 (2012) 452–459, https://doi.org/10.1016/j.conbuildmat.2011.12.073.

[10] M. Hawwash, V. Dörlich, J. Linn, R. Müller, R. Keller, Effective Inelastic Bending Behavior of Multi-Wire Cables Using Finite Elements Accounting forWire Contact, in: Proceedings of the 10th ECCOMAS Thematic Conference on MULTIBODY DYNAMICS, Budapest University of Technology and Economics, Online, 2021, pp. 369–379.

[11] J. Linn, K. Dreßler, Discrete Cosserat Rod Models Based on the Difference Geometry of Framed Curves for Interactive Simulation of Flexible Cables, in: L. Ghezzi, D. Hömberg, C. Landry (Eds.), Math for the Digital Factory, vol. 27, Springer International Publishing, Cham, 2017, pp. 289–319.
[12] H.-J. Kim, D.-H. Lee, K. Yoon, P.-S. Lee, A multi-director continuum beam finite element for efficient analysis of multi-layer strand cables, Comput. Struct. 256 (2021) 106621, https://doi.org/10.1016/j.compstruc.2021.106621.
[13] G. Kastratović, N. Vidanović, V. Bakić, B. Rašuo, On finite element analysis of sling wire rope subjected to axial loading, Ocean Eng. 88 (2014) 480–487, https://doi.org/10.1016/j.oceaneng.2014.07.014.
[14] E. Taghipour, S.S. Vemula, Z. Wang, Y. Zhou, H. Qarib, K. Gargesh, L.M. Headings, M.J. Dapino, S. Soghrati, Characterization and computational modeling of electrical wires and wire bundles subject to bending loads, Int. J. Mech. Sci. 140 (2018) 211–227, https://doi.org/10.1016/j.ijmecsci.2018.03.009.
[15] D. Jungkenn, F. Schneider, F. Andersson, J. Linn, Realistic parameters for dynamic simulation of composite cables using a damped Cosserat rod model, in: ECCOMAS Thematic Conference on Multibody Dynamics, Budapest University of Technology and Economics, 2021, pp. 391–399.
[16] C. Soize, A nonparametric model of random uncertainties for reduced matrix models in structural dynamics, Probab. Eng. Mech. 15 (3) (2000) 277–294, https://doi.org/10.1016/S0266-8920(99)00028-4.
[17] S. Adhikari, Matrix Variate Distributions for Probabilistic Structural Dynamics, AIAA J. 45 (7) (2007) 1748–1762, https://doi.org/10.2514/1.25512.
[18] J.A. Mingo, R. Speicher, Free Probability and Random Matrices, Fields Institute Monographs, vol. 35, Springer, New York, New York, NY, 2017.
[19] C. Soize, Uncertainty Quantification: An Accelerated Course with Advanced Applications in Computational Engineering, Interdisciplinary Applied Mathematics, vol. 47, Springer International Publishing, Cham, 2017.
[20] E.T. Jaynes, Information Theory and Statistical Mechanics, Phys. Rev. 106 (4) (1957) 620–630, https://doi.org/10.1103/PhysRev.106.620.
[21] C. Soize, A comprehensive overview of a non-parametric probabilistic approach of model uncertainties for predictive models in structural dynamics, J. Sound Vib. 288 (3) (2005) 623–652, https://doi.org/10.1016/j.jsv.2005.07.009.
[22] S. Adhikari, A Non-Parametric Approach for Uncertainty Quantification in Elastodynamics, in: 47th AIAA/ASME/ASCE/AHS/ASC Structures, Structural Dynamics, and Materials Conference, American Institute of Aeronautics and Astronautics, Newport, Rhode Island, 2006.
[23] C. Soize, Maximum entropy approach for modeling random uncertainties in transient elastodynamics, J. Acoust. Soc. Am. 109 (2001) 1979–1996, https://doi.org/10.1121/1.1360716.
[24] C. Soize, Random matrix theory for modeling uncertainties in computational mechanics, Comput. Methods Appl. Mech. Eng. 194 (12) (2005) 1333–1366, https://doi.org/10.1016/j.cma.2004.06.038.
[25] S. Adhikari, Wishart Random Matrices in Probabilistic Structural Mechanics, J. Eng. Mech. 134 (12) (2008) 1029–1044, https://doi.org/10.1061/(ASCE)0733-9399(2008)134:12(1029).
[26] N.F. Morris, The use of modal superposition in nonlinear dynamics, Comput. Struct. 7 (1) (1977) 65–72, https://doi.org/10.1016/0045-7949(77)90061-X.
[27] A. Brandt, Noise and Vibration Analysis: Signal Analysis and Experimental Procedures, 1st Edition, Wiley, 2011.
[28] D.J. Ewins, Modal Testing: Theory, Practice, and Application, 2nd Edition, Mechanical Engineering Research Studies, vol. 10, Research Studies Press, Baldock, Hertfordshire, England; Philadelphia, PA, 2000.
[29] C. Shih, Y. Tsuei, R. Allemang, D. Brown, Complex mode indication function and its applications to spatial domain parameter estimation, Mech. Syst. Signal Process. 2 (4) (1988) 367–377, https://doi.org/10.1016/0888-3270(88)90060-X.
[30] T. Kuttner, A. Rohnen, Praxis der Schwingungsmessung: Messtechnik und Schwingungsanalyse mit MATLAB®, Springer Fachmedien, Wiesbaden, Wiesbaden, 2019.
[31] S. Sentpali, Körperschallübertragung gerader und gebogener Schlauchleitungen im Fahrzeugbau, Ph.D. thesis, Technische Universität Kaiserslautern, 2008.
[32] S.S. Rao, Vibration of Continuous Systems, Wiley, Hoboken, N.J, 2007.